Catalysis Today xxx (xxxx) xxx–xxx

Contents lists available at ScienceDirect

Catalysis Today

journal homepage: www.elsevier.com/locate/cattod

High utilization of methanol in toluene methylation using MFI zeolite nanosponge catalyst

Changq Lee[a], Seungjun Lee[a,b], Wookdong Kim[b,*], Ryong Ryoo[a,b,*]

[a] Department of Chemistry, Korea Advanced Institute of Science and Technology (KAIST), Daejeon 34141, Republic of Korea
[b] Center for Nanomaterials and Chemical Reactions, Institute for Basic Science (IBS), Daejeon 34141, Republic of Korea

ARTICLE INFO

Keywords:
MFI zeolite nanosponge
Surfactant-directed zeolite
Hierarchical zeolite
Toluene methylation
Methanol utilization

ABSTRACT

A highly mesoporous MFI zeolite nanosponge, which was composed of a disordered assembly of 2.5-nm thick zeolite frameworks, was synthesized using a meso- and micropore dual structure-directing surfactant. The zeolite nanosponge was investigated as a catalyst for toluene methylation by methanol. The results showed remarkably high toluene conversion and xylene yield, in comparison with the bulk zeolite counterparts. The high catalytic performance was attributed to the suppression of side reactions that could convert methanol to linear hydrocarbons. This suppression can be attributed to the fact that the dealkylation of polymethylbenzenes, which must take place before linear hydrocarbon formation, did not occur significantly in the zeolite nanosponge as compared to the case of bulk zeolites. In addition to the aforementioned high performance, the MFI zeolite nanosponge was also superior to the bulk MFI in terms of catalytic longevity.

1. Introduction

Benzene, toluene, and xylene (BTX) are basic raw materials for various petrochemical products [1]. One of the largest sources of BTX is from the catalytic reforming of heavy naphtha. However, in this process, toluene is overproduced relative to current market demand. The surplus toluene should be converted to a more valuable xylene via transalkylation or methylation processes [1–3]. Among the toluene-to-xylene conversion processes, methylation using methanol [2–5] has been a focus of attention in recent years after methanol became available at low cost from shale gas processing [6]. In recent decades, the toluene methylation process has been extensively studied using various zeolite catalysts with common names, such as Y [7], ZSM-5 [3,5,8,9], mordenite [5,9], beta [5,9], MCM-22 [10], and SSZ-33 [3]. Among the investigated zeolites, high silica ZSM-5 turned out to be the most suitable catalyst. The main feature of this zeolite is its pores, which are composed of 10-membered oxygen rings (*i.e.*, 10-MR). The 10-MR pores are wide enough for the first alkylation reaction to take place, but cause steric hindrance to further reactions to polymethylbenzenes (*e.g.*, hexamethylbenzene). Thus, high xylene selectivity is an advantage of these 10-MR zeolites [5,9]. Furthermore, the narrow 10-MR zeolite pores exhibit shape selectivity for *p*-xylene over the *o*- and *m*- isomers. Since *p*-xylene is more valuable than *o*- and *m*-xylenes, there have been very extensive studies on ways to increase the shape selectivity [11–13]. These 10-MR zeolites were modified in various ways with oxides of boron, magnesium, silicon, and phosphorus to achieve high *p*-xylene selectivity. However, these modifications led to a decreased toluene conversion owing to the inherent trade-off relationship, which implied a low first-pass yield and high recycling flow in the conventional zeolite-based catalytic processes. Consequently, this strategy could increase both the investment and operational costs and reduce the economics and efficiency of aromatic plants.

In the present work, we focus our attention on the toluene methylation approach that pursues high toluene conversion and xylene yield rather than high *p*-xylene selectivity. We note that this methylation process is normally carried out in a temperature range of 623 ~ 723 K. If we use a conventional ZSM-5 zeolite as a catalyst under such high-temperature conditions, the toluene conversion is usually less than 40%. This low toluene conversion is attributed to the consumption of methanol in side reactions [5,9,14], typically producing multi-methylated toluenes (*e.g.*, tri- and tetra-methylbenzenes) and linear hydrocarbons (*e.g.*, ethylene and propylene). Ahn et al. [5] investigated the methanol usage for side reactions using medium pore (10-MR) zeolites (*e.g.*, ZSM-5 and ZSM-11) and large pore (12-MR) zeolites (*e.g.*, MOR and BEA). They showed that the low production of multi-methylated toluenes and the high yield of linear hydrocarbons in ZSM-5 zeolites are due to a pore size effect. They also reported the effect of the zeolite crystal size on methanol usage, but predicted that the effect would be modest for the zeolite crystals of < 100 nm.

ZSM-5 zeolite is built with an MFI structure type aluminosilicate

* Corresponding authors.
E-mail addresses: wdkim@kaist.ac.kr, rryoo@kaist.ac.kr (R. Ryoo).

http://dx.doi.org/10.1016/j.cattod.2017.09.056
Received 1 June 2017; Received in revised form 20 August 2017; Accepted 29 September 2017

framework. Typically, the MFI zeolite is synthesized with tetrapropylammonium (TPA) cations as a structure-directing agent (SDA). However, the ZSM-5 zeolite synthesized with TPA normally exhibits bulk crystal morphology. To decrease the zeolite crystal thickness, Ryoo and co-workers developed a synthesis method using a surfactant functionalized with a diammonium group [15]. The crystal thickness obtained in this manner was only 2.5 nm thick, which was very close to a unit-cell parameter along the crystal *b*-axis (*i.e.*, 2.0 nm). Moreover, when the synthesis was seeded, MFI zeolite nanosheets were obtained as a self-assembled highly mesoporous nanosponge exhibiting a sharp distribution of mesopore diameters centered at 3.5 nm [16]. The zeolite was called a MFI zeolite nanosponge. MFI zeolite nanosheets have been reported to show very rapid molecular diffusion under various catalytic reaction conditions [15–21]. Due to the rapid diffusion, the zeolite nanosheets exhibited a high isomer selectivity in *n*-heptane hydroisomerization and an extremely long catalyst lifetime in methanol-to-hydrocarbon (MTH) reactions.

In the present study, the catalytic properties of mesoporous MFI zeolite nanosponge in toluene methylation were investigated. MFI zeolites having crystal thickness of 20 nm and 200 nm were synthesized and used to compare the catalytic properties of the nanosponge. The results of this investigation indicated that the MFI zeolite nanosponge with 2.5-nm framework thickness did indeed attain a remarkably a high toluene conversion and xylene yield as compared to bulk MFI zeolite counterparts. Moreover, the MFI zeolite nanosponge exhibited a much longer catalytic lifetime than that of the bulk MFI zeolites. We report these results in the present paper.

2. Experimental

2.1. Zeolite synthesis and characterization

MFI zeolite nanosponge was synthesized with a $[C_{18}H_{37}–N^+(CH_3)_2–C_6H_{12}–N^+(CH_3)_2–C_6H_{13}][Br^-]_2$ surfactant as reported elsewhere (see Supplementary information S1 for details) [16]. Nanocrystalline and bulk MFI zeolites were synthesized using $[C_3H_7–N^+(CH_3)_2–C_6H_{12}–N^+(CH_3)_2–C_3H_7][Br^-]_2$ and TPAOH, respectively [21,22]. The zeolite samples were calcined in air to remove the organic SDAs at 823 K. The calcined zeolites were ion exchanged with NH_4^+ in an aqueous solution of 1 M NH_4NO_3, and calcined again in air at 823 K to convert the exchanged NH_4^+ ions to H^+. The H^+-form zeolites were investigated as a toluene methylation catalyst, and characterized by scanning electron microscopy (SEM, FEI Nova 230), transmission electron microscopy (TEM, Tecnai G2 F30), powder X-ray diffraction (XRD, Rigaku Multiflex diffractometer), and argon adsorption-desorption (Quantachrome autosorb iQ2). The Si/Al atomic ratio was analyzed by inductively coupled plasma-atomic emission spectroscopy (ICP-AES, Perkin Elmer OPTIMA 4300 DV). The acidic properties were analyzed by solid-state ^{27}Al and ^{31}P nuclear magnetic resonance spectroscopy (NMR, Bruker AVANCE400WB). The experimental details of the characterization were the same as described elsewhere [16,17,22,23].

2.2. Catalytic reaction measurements

The toluene methylation reaction was carried out in a continuous-flow, fixed-bed, stainless-steel reactor (inner diameter = 6 mm) under N_2 at atmospheric pressure. The temperature at the catalyst was measured using a K-type thermocouple placed in the reactor. The amount of powdered catalyst was varied from 0.05 to 0.21 g. For a small amount of catalyst ($\leq$ 0.10 g), the zeolite catalysts were diluted with inert silicon carbide to avoid channeling of the reactant gas [24,25]. Prior to the reaction, the catalyst was activated under a N_2 atmosphere for 2 h at 773 K. After cooling to the preset reaction temperature (between 473 and 773 K), an equimolar mixture of methanol and toluene was fed into the reactor via a HPLC pump (LabAlliance, Series III). The weight hourly space velocity (WHSV) was varied from 7.1 to 115 h^{-1} with respect to the toluene. The flow rate of the N_2 carrier gas was controlled using a mass-flow controller, maintaining a N_2/(toluene + methanol) molar ratio of 4. Catalyst performance was measured at 30 min, after feeding of the reactants started. The product distribution was analyzed with an online gas chromatograph (GC, Younglin, Acme-6000) equipped with a flame ionization detector. Two fused-silica capillary GC columns were used: 30 m × 0.32 mm GS-GasPro for the separation of the product stream and 30 m × 0.53 mm × 40 μm HP-PLOT/Q for methanol detection. The lifetime of the catalysts was investigated at 673 K and 31 h^{-1} for prolonged reaction time (> 20 h). At the same conditions, the zeolite catalysts were collected after 16 h and the coke content in the catalysts was analyzed by thermogravimetric analysis (TA Instrument, TGA Q500).

Toluene disproportionation and ethylbenzene dealkylation were performed using the same stainless-steel reactor as employed for toluene methylation. The details in the measurement of these reactions were described in the Supplementary information S2.

3. Results and discussion

3.1. Physicochemical characterization of the investigated catalysts

Three MFI zeolite samples were synthesized in the present work, and compared to each other as catalysts for toluene methylation using methanol. One sample was an MFI zeolite exhibiting the morphology of a nanosponge, in which 2.5-nm thick MFI nanosheets were interconnected in a disordered manner to support mesopores. The nanosheets were rigidly interconnected through their intergrowths which developed during the hydrothermal synthesis process. This nanosponge sample is denoted as 'NS-2.5′ according to the nanosheet thickness. The other two samples were ZSM-5 zeolites with nanocrystalline (20 nm in average crystal thickness) and bulk crystalline morphologies (200 nm in average thickness). The two zeolite samples are denoted as 'NC-20′ and 'B-200′, respectively, according to their crystal morphologies and thicknesses. These zeolite samples were synthesized and characterized by the same procedures described elsewhere [16,17,22,23]. The results of their characterizations are summarized in Table 1. The details of these results are only briefly described in the remainder of this section.

Table 1
Physicochemical properties of the MFI zeolite samples.

Samples	Si/Al[a]	S_{BET}(m^2 g^{-1})[b]	S_{ext}(m^2 g^{-1})[c]	Total acid sites titrated with TMPO (μmol g^{-1})		External acid sites titrated with TBPO (μmol g^{-1})	
				A_{total}[d]	$A_{total,strong}$[e]	A_{ext}[f]	$A_{ext,strong}$[g]
NS-2.5	41	610	380	348	143	133	38
NC-20	39	470	110	354	189	35	15
B-200	41	410	40	364	182	17	4

[a] Si/Al mole ratio determined by elemental analysis using ICP-AES. [b] BET surface area from Ar adsorption in the relative pressure range of 0.1–0.3. [c] External surface area according to the *t*-plot method. [d] A_{total} is the concentration of total acid sites, corresponding to resonance peaks at 86, 76, 68, and 66 ppm for TMPO titrated zeolites. [e] $A_{total,strong}$ is the concentration of strong acid sites, corresponding to the peaks at 86 and 76 ppm. [f] A_{ext} is the concentration of external acid sites, corresponding to the peaks at 92, 74, and 72 ppm for TBPO titrated zeolite samples. [g] $A_{ext,strong}$ is the concentration of strong external acid sites, corresponding to the peak at 92 ppm.

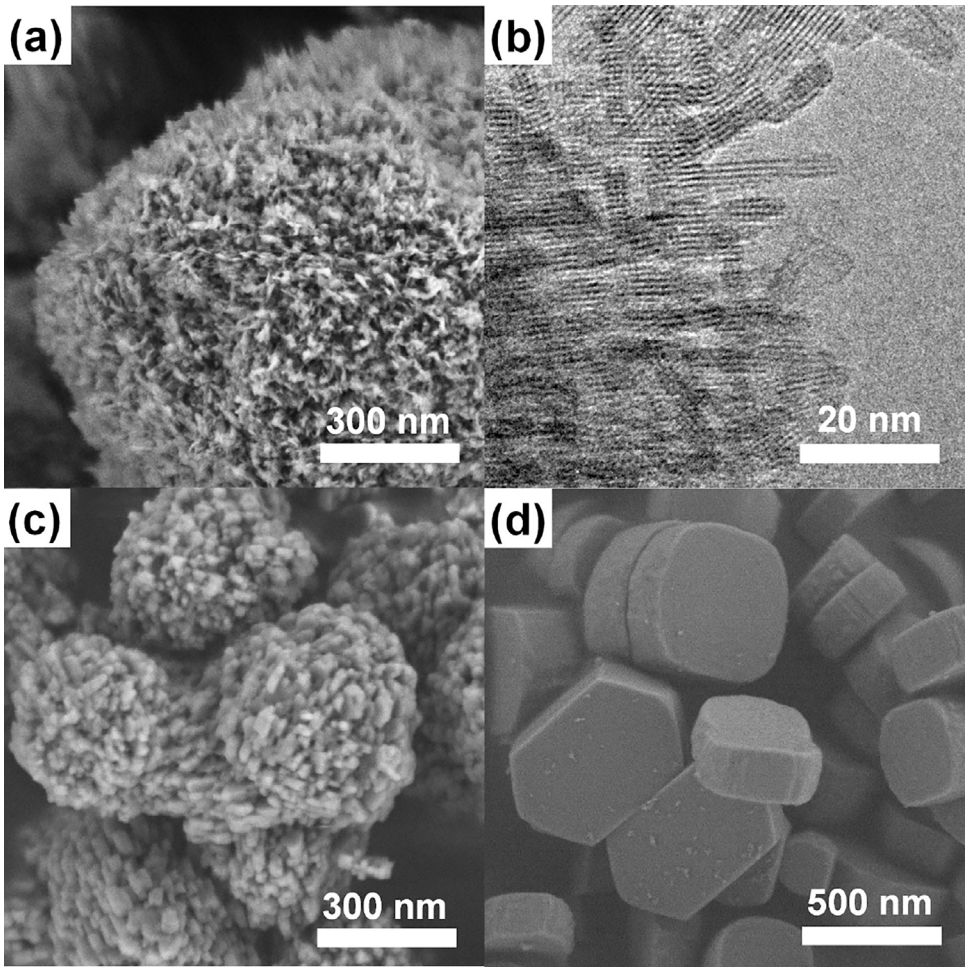

Fig. 1. Representative SEM images for (a) NS-2.5, (c) NC-20, and (d) B-200 samples. For the NS-2.5 sample, (b) a high resolution TEM image is also shown.

Fig. 1 shows representative SEM and TEM images of the three zeolite samples. As shown in Figs. 1a and 1b, the NS-2.5 sample consisted of sponge-like mesoporous particles. The frameworks of the porous particles were MFI zeolite nanosheets of 2.5 nm thickness. Each of the nanosheets corresponded to a thickness of 3 pentasil layers. The zeolite nanosheets were rigidly interconnected to the mesoporous sponge-like morphology. On the other hand, as shown in Fig. 1c, the NC-20 sample also had a nanosponge-like morphology, but it consisted of aggregated nanocrystals. The crystal thickness (*i.e.*, diameter in the thinnest dimension) of the individual nanocrystals was approximately 20 nm. Fig. 1d shows that the B-200 sample exhibited bulk crystalline morphology. The crystal thickness was distributed over a range of 150 ~ 250 nm. The MFI-type structure of zeolite samples was confirmed by XRD (Supplementary information Fig. S1a) [16].

The porous textural properties of the zeolite samples were analyzed with argon adsorption isotherms at 87 K (Supplementary information Fig. S1b), and the result is given in Table 1. The specific surface area was determined by the Brunauer-Emmett-Teller (BET) equation, and the external surface area was analyzed by the *t*-plot method. The results obtained in this manner showed that NS-2.5 possessed a high external surface area of 380 $m^2\ g^{-1}$. This value was nine-times larger than that of B-200 (40 $m^2\ g^{-1}$). In addition, the mesopore size distribution was analyzed according to the Barrett-Joyner-Halenda method. The result for NS-2.5 exhibited a narrow peak centered at 4 nm (Supplementary information Fig. S2). This result confirmed that the nanosponge sample had uniform mesopore diameters, despite their disordered arrangement [16].

Elemental analysis using ICP-AES indicated that all three samples were prepared with very similar Si/Al ratios (40 ± 1) (Table 1). The solid-state ^{27}Al MAS NMR spectra of the zeolite samples revealed that most of the Al atoms were incorporated into the zeolite frameworks with tetrahedral coordination (Supplementary information Fig. S3). The concentration of Brönsted acid sites of the zeolite samples was quantitatively analyzed by ^{31}P MAS NMR spectroscopy using trimethylphosphine oxide (TMPO) and tributylphosphine oxide (TBPO) as basic titrants [23,26]. The kinetic diameters of TMPO and TBPO are 0.55 nm and 0.82 nm, respectively. In this NMR method, note that the TMPO probe molecule is assumed to be small enough to reach the internal acid sites that are located inside the micropores, as well as the external acid sites located on the mesopore walls. Hence, the TMPO-based result is regarded as the total acid site (internal + external acid sites) concentration. When TMPO is substituted with a bulkier molecule, TBPO, the probe molecule cannot enter the apertures of the MFI micropores. Hence, the ^{31}P NMR analysis using TBPO can selectively detect the external acid sites.

In the NMR spectra shown in Fig. 2, several resonance peaks (86, 76, 68, and 66 ppm for TMPO and 92, 74, and 72 ppm for TBPO) corresponding to phosphine oxides adsorbed on the acid sites of zeolites are observed. The concentration of acid sites corresponding to each resonance peak was calculated from the area of resonance peak in combination with the P content of phosphine oxide adsorbed zeolites. The concentration of total acid sites, which was the sum of the concentrations of all acid sites, was 348 μmol g^{-1} for NS-2.5, 354 μmol g^{-1} for NC-20, and 364 μmol g^{-1} for B-200 (Table 1). The concentration of total acid sites with strong acidity was the sum of the concentrations of acid sites corresponding to the resonance peaks at 86 and 76 ppm for the TMPO titration. NS-2.5 possessed 143 μmol g^{-1} of total strong acid sites and NC-20 and B-200 had 189 μmol g^{-1}, and 182 μmol g^{-1},

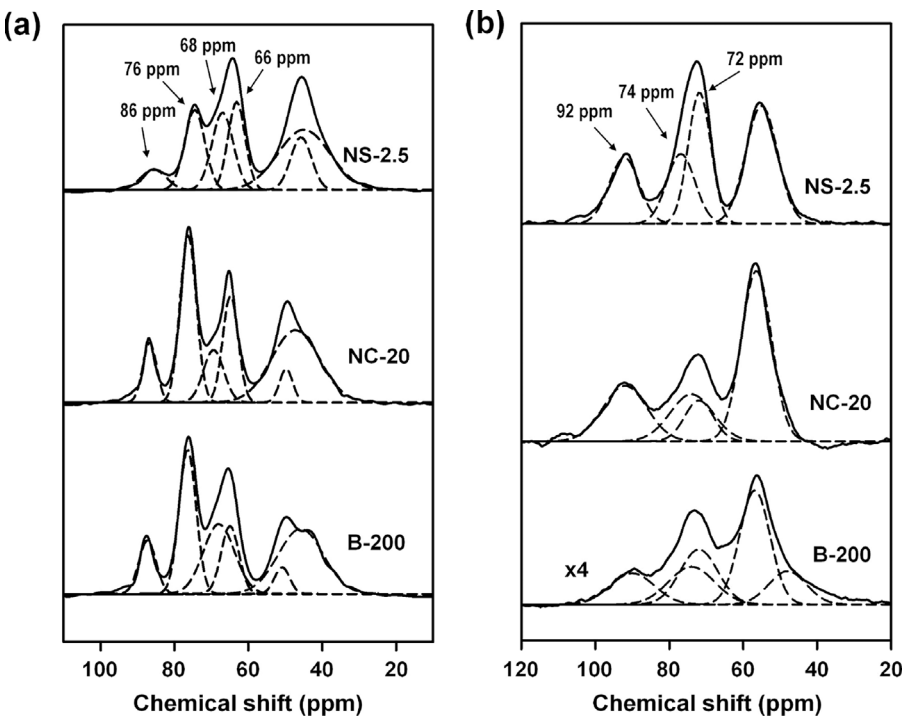

Fig. 2. ^{31}P NMR spectra of (a) TMPO and (b) TBPO adsorbed MFI zeolite samples. All spectra are collected with the same number of acquisition, reduced to the same sample mass, and then plotted on the absolute intensity scale. Dotted line in the spectra indicates the resonance peaks deconvoluted by the Gaussian method.

respectively. The concentration of strong external acid sites, corresponding to the NMR peak at 92 ppm in the TBPO titration, was 38 μmol g^{-1} for NS-2.5 but only 4 μmol g^{-1} in the case of B-200.

3.2. Toluene methylation results

3.2.1. Product distribution for toluene methylation at approximately 80% methanol conversion

In the present work, we performed a toluene methylation reaction at various reaction temperatures (473 to 773 K) and WHSV values (7.1 to 115 h^{-1}) using MFI zeolite catalysts. To compare the reaction results at a methanol conversion of 80%, the reaction conditions were selected with a fixed reaction temperature of 673 K and different WHSVs for each catalyst. Table 2 shows the product distribution at these reaction conditions. As the distribution results show, the product stream contained various hydrocarbons such as $C_1 \sim C_5$ aliphatics, toluene, xylenes, trimethylbenzenes, tetramethylbenzenes, and other C_{9+} aromatics (*e.g.*, ethylmethylbenzenes). Xylenes are produced through the reaction of toluene with a methanol molecule, and polymethylbenzenes (aromatics larger than xylenes) are formed via consecutive reactions with additional methanol molecules. On the other hand, various C_{2+} alkenes were generated by dealkylation of polymethylbenzenes and subsequent olefin methylation [5]. In particular, C_{6+} olefins can be converted to aromatic compounds through aromatization with concomitant production of $C_2 \sim C_4$ paraffins via hydrogen transfer reaction [27]. The product distribution in Table 2 indicates that both aromatic methylation and olefin methylation occurred to a significant extent. However, negligible amounts of C_{6+} aliphatics and $C_2 \sim C_4$ paraffins were present in the product stream. This indicated that the production of aromatics from olefins was not considerable during the toluene methylation reaction over the MFI zeolite catalysts.

As shown in the product distributions, the yields of hydrocarbon products varied remarkably according to the thickness of the MFI zeolite catalyst. The NS-2.5 catalyst exhibited the lowest content of $C_1 \sim C_5$ hydrocarbons (1.1 wt%) among the three investigated catalysts while the content of methylated aromatic products was highest: 32.6 wt% xylene, 10.2 wt% trimethylbenzenes, and 3.2 wt% tetramethylbenzenes. From the distribution, methanol conversion, toluene conversion, xylene selectivity, xylene yield, and *p*-xylene selectivity were evaluated and the results are shown in the last five rows of Table 2. For all catalysts, the methanol conversion calculated from the distribution in Table 2 was similar within 80.2 ± 0.5%. Toluene conversion is the percentage of converted toluene over toluene reactant and xylene selectivity is the percentage of xylene over the aromatic products. As shown in Table 2, NS-2.5 exhibited the highest toluene conversion, 46.2%, among the investigated MFI zeolite catalysts. The

Table 2
Product distributions for the three MFI zeolite catalysts obtained at approximately 80% methanol conversion.

	NS-2.5	NC-20	B-200
Reaction temperature (K)	673	673	673
WHSV (h^{-1})	85	29	14
Product distribution (wt%)			
methanol	5.6	5.7	5.9
dimethyl ether	1.6	1.3	1.2
methane	0.2	0.2	0.2
ethane	– [a]	–	–
ethylene	0.4	1.1	2.4
propane	–	0.1	0.2
propylene	0.4	0.9	1.9
butane	–	–	0.1
butylene	0.1	0.4	0.7
C_5 aliphatics	–	0.2	0.3
C_{6+} aliphatics	–	–	–
toluene	45.1	51.5	62.0
p-xylene[b]	8.1	6.6	4.7
m-xylene	15.9	14.3	10.4
o-xylene	8.6	6.7	4.6
trimethylbenzenes	10.2	8.6	3.8
tetramethylbenzenes.	3.2	2.0	1.1
other C_{9+} aromatics	0.6	0.4	0.5
methanol conversion (%)	80.7	80.2	79.8
toluene conversion (%)	46.2	38.5	25.4
xylene selectivity (%)	73.0	74.4	80.9
xylene yield (%)	33.7	28.6	20.5
p-xylene selectivity (%)	24.8	23.9	23.9

[a] '–' indicates that the content of component is less than 0.1 wt%. [b] The amount of *p*-xylene and other xylene isomers was determined using a 60 m × 0.32 mm × 0.5 μm HP INNOWax GC column.

toluene conversion decreased as the crystal thickness of the zeolite catalyst increased. In contrast, the xylene selectivity showed an opposite trend to that of the toluene conversion. The xylene selectivity for NS-2.5 was 73.0% while that for B-200 was 80.9%. The low selectivity to xylene for the NS-2.5 catalyst was due to the considerable production of multi-methylated aromatics. Despite lowering the xylene selectivity in toluene methylation, polymethylbenzenes are not useless byproducts because they can be recycled into xylenes by means of the transalkylation process [1]. Without considering this, the difference in xylene selectivity among the three catalysts seemed to be modest. Moreover, the xylene yield calculated by multiplying the toluene conversion and xylene selectivity was much higher in NS-2.5 (33.7%) than in B-200 (20.5%).

3.2.2. Methanol utilization in toluene methylation over MFI zeolite catalysts

As Table 2 shows, the methanol conversion for the MFI zeolite catalysts was higher than the toluene conversion. This difference in conversion was due to the utilization of a considerable amount of methanol in the side reactions that could produce $C_1 \sim C_5$ linear hydrocarbons and polymethylbenzenes rather than in the reaction with toluene to produce the target molecules, xylenes. Therefore, to better understand the high toluene conversion and xylene yield in the NS-2.5, it is important to analyze the methanol utilization for the side reactions. For convenience, methanol utilization during the toluene methylation was divided into four types as follows: methanol for the formation of dimethyl ether (DME) and linear hydrocarbons (LH), multi-methylation (MuM) of toluene, and mono-methylation (MoM) of toluene. DME is formed via condensation of two methanol molecules. Note that it can be reversibly hydrated to methanol under typical reaction conditions and can be utilized as an alkylating agent [5]. For the calculation of methanol utilization, it was assumed that one methanol molecule is consumed to produce one xylene molecule via the mono-methylation reaction, two or more methanol molecules per polymethylbenzenes. With these assumptions, the number of methanol molecules utilized for MuM and MoM of toluene can be calculated using each of the product yields in Table 2. The remainder of the converted methanol can be considered as lost for LH formation.

Fig. 3 shows the methanol utilization (%) calculated in the aforementioned manner. As the results show, all catalysts exhibited the similar methanol utilization for DME (7.0 ~ 9.8%). The methanol utilization for MuM and MoM of toluene increased remarkably together as the crystal thickness decreased. The nanosponge catalyst (NS-2.5) exhibited the highest methanol utilization for MoM (43.3%) and MuM (35.7%) reactions, with the lowest loss (11.1%) attributed to the LH formation. On the other hand, B-200, which has the lowest xylene yield, exhibited the highest amount of methanol utilization for the LH formation (55.2%). As shown in Table 2, the major components of linear hydrocarbons in the product distributions are ethylene and propylene that were produced by dealkylation of polymethylbenzenes. Moreover, the remaining linear hydrocarbons are formed via methylation of ethylene and propylene. Thus, the rate of dealkylation is the most important factor determining the amount of methanol consumed in the formation of linear hydrocarbons.

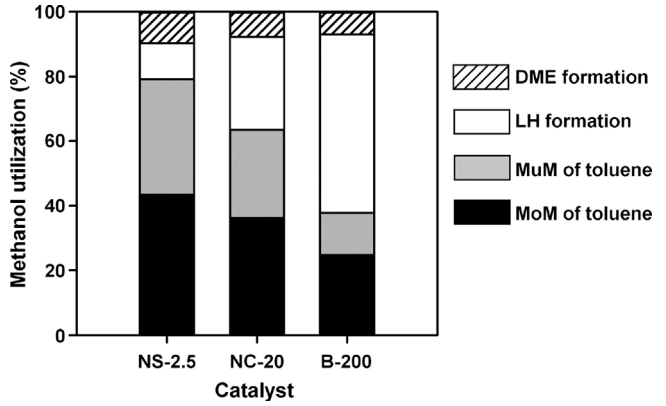

Fig. 3. Methanol utilization during toluene methylation over the three MFI zeolite catalysts: methanol for the formation of dimethyl ether (DME) and linear hydrocarbons (LH), multi-methylation (MuM) of toluene, and mono-methylation (MoM) of toluene. The utilization was calculated from the product distribution obtained at approximately 80% methanol conversion (Table 2).

To compare the dealkylation rate of the three MFI zeolite catalysts, we selected toluene as a model chemical and measured the toluene conversion in the toluene disproportionation reaction. In the reaction, the methyl group of toluene was dealkylated and subsequently moved to another toluene. The toluene conversion measured at 723 K and 2 h^{-1} decreases in the order of B-200 (3.6%) > NC-20 (2.4%) > NS-2.5 (1.0%). At such low conversion levels (< 5%), the conversion is considered to be proportional to the reaction rate. Hence, the rate of the disproportionation reaction was significantly low for NS-2.5. In addition, for the ethylbenzene dealkylation performed at 673 K and 5 h^{-1}, we obtained a similar trend of catalytic activity to the case of toluene disproportionation: The ethylbenzene conversion decreased in the order of B-200 (21.4%) > NC-20 (18.3%) > NS-2.5 (12.2%). From the results of toluene disproportionation and ethylbenzene dealkylation, it can be expected that the dealkylation reaction occurred less often in NS-2.5 and thus, the methanol was less consumed in the LH formation and instead, was more effectively utilized in toluene methylation to xylenes.

The low dealkylation rate of NS-2.5 can be explained by the relatively small specific micropore volume and less strong internal acids (see Table 1) compared to that of bulk zeolite counterparts. According to the mechanism studies for the MTO reaction [28,29], light hydrocarbons are produced from the dealkylation of intermediate polymethylbenzenes via various methylcyclopentenyl cations that can be considerably stabilized in confined 10-MR MFI zeolite micropores. On the other hand, such spatial confinement effects are expected to be less significant in larger micropores of 12-MR zeolites and the dealkylation reaction is observed to be less prevalent [5]; thus, at open external surface acid sites, the dealkylation reaction would occur much less frequently, compared to that at the internal acid sites of the zeolites. According to Table 1, NS-2.5 has the largest number of external acid sites and the lowest number of internal acid sites, among the present MFI zeolites. Specifically, the strong internal acid concentration of NS-2.5, which can be calculated by subtracting the concentration of the external strong acid sites from that of total strong acid sites, was 105 μmol g^{-1}, which is significantly lower than that of the bulk zeolite counterparts (174 μmol g^{-1} for NC-20 and 178 μmol g^{-1} for B-200).

In addition, the diffusion of bulky polymethylbenzenes, which are prone to be dealkylated, is highly restricted when they are generated inside the micropore channels of MFI zeolites during the toluene methylation. Therefore, the residence time of polymethylbenzenes in the zeolite is quite long and thus the probability of dealkylation catalyzed by the acid sites is high. The residence time can be reduced by decreasing the diffusion path length in the micropores. Therefore, for MFI nanosponge of 2.5 nm-thickness, the polymethylbenzenes can escape rapidly before being dealkylated into short olefins. In addition, the NS-2.5 zeolite nanosponge possesses the highest concentration of external acid sites (38 μmol g^{-1}) among the MFI zeolite catalysts (see Table 1). At the external surface, the molecular diffusion is much faster than inside the micropores, and hence the polymethylbenzenes can leave readily from the surface to the gas phase [30].

3.2.3. Toluene methylation at various reaction temperature and WHSV

In order to investigate the effect of reaction temperature and WHSV, the reaction temperatures were changed from 473 to 773 K at a fixed WHSV of 7.1 h^{-1} (with respect to toluene) and WHSV was varied from 7.1 to 115 h^{-1} at a fixed temperature of 673 K. The methanol conversion, toluene conversion, xylene selectivity, and xylene yield were calculated as the aforementioned manner (see Section 3.2.1.). The yield

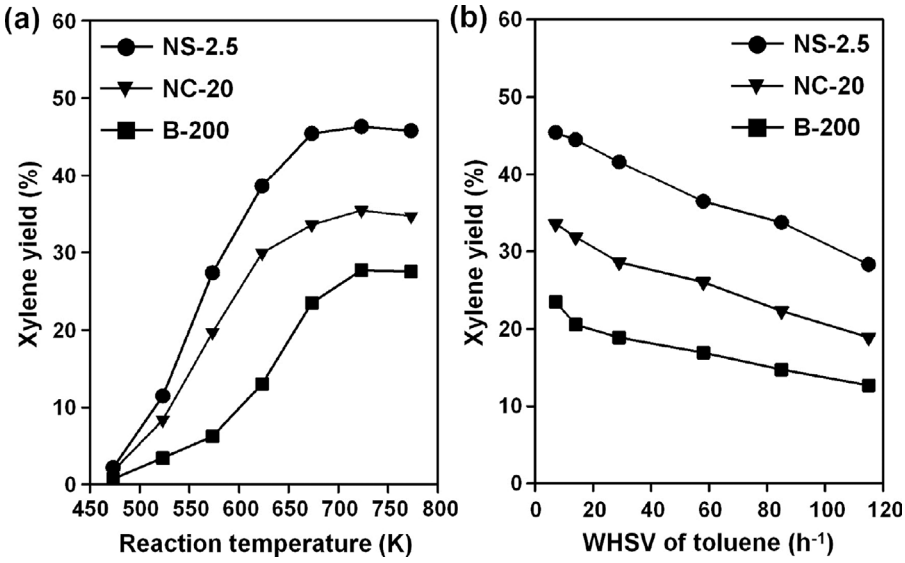

Fig. 4. Xylene yield for the three MFI zeolite catalysts plotted as a function of (a) the reaction temperature at a fixed WHSV of 7.1 h^{-1} and (b) the WHSV at a fixed reaction temperature of 673 K. (Reaction conditions: temperature range = 473–773 K; WHSV of toluene = 7.1–115 h^{-1}).

of target products, xylenes, was described in Fig. 4. and other results were depicted in Fig. S4 in the Supplementary information. The temperature-vs.-yield plots for all catalyst samples showed a gradual increase with increasing temperatures from 473 to 723 K, and then a slight decrease upon any further increases. Thus, the catalyst samples all exhibited a maximum yield at about 723 K. When compared at a given temperature, the xylene yield increased as the zeolite crystal thickness decreased throughout the whole investigated temperature range. At the maximum point at 723 K, the NS-2.5 zeolite exhibited the highest xylene yield of 46.3% while the xylene yield for the NC-20 and B-200 zeolites was 35.4% and 27.7%, respectively. A plot of the xylene yield from each catalyst as a function of the WHSV over the range of 7.1 to 115 h^{-1} at a fixed temperature of 673 K showed that the NS-2.5 had the best catalytic performance (Fig. 4b). The xylene yield curve for NS-2.5 displayed a linear decrease from low to high WHSV. The other samples exhibited a similar decreasing behavior, but the yields were lower. The toluene conversion plot in Figs. S4b and S4e exhibited similar behavior with those of the xylene yield, indicating a maximum of 71.6% with NS-2.5 at 723 K. On the other hand, the xylene selectivity showed an inverse correlation with the toluene conversion, implying a pronounced production of multi-methylated benzenes with increased toluene conversion. A commercial zeolite (CBV8014, Si/Al = 40) was transformed into H^+-form and evaluated as a reference catalyst for toluene methylation (see Supplementary information Fig. S5).

3.2.4. Catalytic lifetime in toluene methylation

For the toluene methylation, the deactivation of the MFI zeolite catalysts was investigated at reaction condition of 673 K and 31 h^{-1}. Fig. 5 shows the variation in toluene conversion measured at this reaction condition with time on stream (TOS). As shown in this figure, the toluene conversion for the NS-2.5 catalyst was 60.8% at the beginning of the catalytic reaction (*i.e.*, 0.5 h). The conversion then decreased slowly and became 28.0% after 125 h. In contrast, the toluene conversion dropped from 38.1% to 8.9% at 50 h for the NC-20, and for the B-200 catalyst, the toluene conversion was only 22.6% at 0.5 h and decreased rapidly to 4% within 16 h. In contrast with the toluene conversion, the xylene selectivity of NS-2.5 was almost constant throughout the deactivation test.

The NS-2.5 catalyst exhibited approximately three-fold higher initial activity and much longer catalytic lifetime than the B-200 catalyst. A long catalytic lifetime of the zeolite nanosheets has also been reported for MTH reactions [15,19], in which the zeolite catalyst was deactivated by a deposition of coke species that were formed via polymerization of side products (*i.e.*, coke precursors). Kim et al.

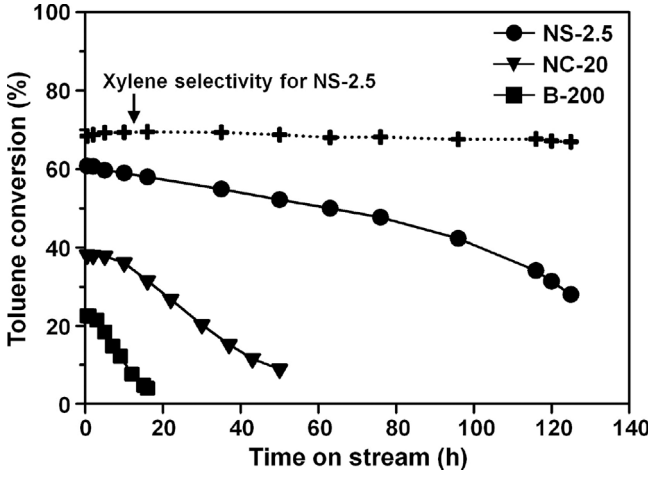

Fig. 5. Variation of toluene conversion for the MFI zeolite catalysts with time on stream. (Reaction condition: reaction temperature = 673 K, WHSV of toluene = 31 h^{-1}). Variation of xylene selectivity for NS-2.5 was also provided.

attributed the slow deactivation of the zeolite nanosheets to the fact that coke precursors can escape rapidly through the extremely thin zeolite crystals before they can be converted to coke [19]. During the toluene methylation, most of the reactions that take place at the catalysts are very similar to those occurring in the MTH reactions, and hence it can be suggested that the present zeolite catalysts were deactivated via a similar route for MTH reactions. Therefore, the slow deactivation and long catalytic lifetime of the zeolite nanosponge could be attributed to rapid diffusion of coke precursors on the zeolites. At 16 h of TOS, the coke content in the NS-2.5 (0.028 g g^{-1}) was remarkably small compared to that in the NC-20 (0.058 g g^{-1}) and B-200 (0.071 g g^{-1}).

4. Conclusions

In the present work, we discovered that an MFI zeolite nanosponge of 2.5-nm thickness exhibited higher toluene conversion and xylene yield than bulk MFI zeolites of 20-nm and 200-nm thickness. The high catalytic performance of the zeolite nanosponge was attributed to the lower consumption of methanol in the side reactions, such as the formation of linear hydrocarbons, and instead higher utilization of methanol for toluene methylation to xylene. During the toluene methylation, linear hydrocarbons were formed by the dealkylation of

polymethylbenzenes into short olefins and subsequent olefin methylation of such short olefins. We speculated that the dealkylation of polymethylbenzenes did not occur considerably in the nanosponge as compared to bulk zeolites. This can be explained by the low concentration of strong internal acid sites that could readily catalyze the dealkylation of polymethylbenzenes. In addition, short micropore channels and a high contribution of external acid sites can cause rapid escape of molecules from acid sites, and therefore can suppress the dealkylation of polymethylbenzenes. This rapid escape of molecules is also known to suppress coke formation by enabling the rapid escape of coke precursors, which consequently enhances catalytic lifetime. The present investigation revealed that the zeolite nanosponge has advantages as a catalyst for small molecular reactions occurring at the acid sites both inside micropores and on their external surfaces. These advantages can be extended to other nanostructured zeolites and various catalytic alkylation reactions.

Acknowledgements

This work was supported by IBS-R004-D1.

Appendix A. Supplementary data

Supplementary data associated with this article can be found, in the online version, at http://dx.doi.org/10.1016/j.cattod.2017.09.056.

References

[1] T.C. Tsai, S.B. Liu, I. Wang, Appl. Catal. A Gen. 181 (1999) 355–398.
[2] A. Baduraig, T. Odedairo, S. Al-Khattaf, Top. Catal. 53 (2010) 1446–1456.
[3] T. Odedairo, R.J. Balasamy, S. Al-Khattaf, Ind. Eng. Chem. Res. 50 (2011) 3169–3183.
[4] I. Hill, A. Malek, A. Bhan, ACS Catal. 3 (2013) 1992–2001.
[5] J.H. Ahn, R. Kolvenbach, S. Al-Khattaf, A. Jentys, J.A. Lercher, ACS Catal. 3 (2013) 817–825.
[6] D.A. Wood, C. Nwaoha, B.F. Towler, J. Nat. Gas. Sci. Eng. 9 (2012) 196–208.
[7] T. Yashima, H. Ahmad, K. Yamazaki, M. Katsuta, N. Hara, J. Catal. 16 (1970) 273–280.
[8] D.V. Vu, M. Miyamoto, N. Nishiyama, Y. Egashira, K. Ueyama, Catal. Letters 127 (2009) 233–238.
[9] Ø Mikkelsen, P.O. Rønning, S. Kolboe, Microporous Mesoporous Mater. 40 (2000) 95–113.
[10] Z. Zhu, Q. Chen, W. Zhu, D. Kong, C. Li, Catal. Today 93-95 (2004) 321–325.
[11] D.V. Vu, M. Miyamoto, N. Nishiyama, Y. Egashira, K. Ueyama, J. Catal. 243 (2006) 389–394.
[12] M. Ghiaci, A. Abbaspur, M. Arshadi, B. Aghabarari, Appl. Catal. A Gen. 316 (2007) 32–46.
[13] J.L. Sotelo, M.A. Uguina, J.L. Valverde, D.P. Serrano, Ind. Eng. Chem. Res. 32 (1993) 2548–2554.
[14] Y. Bi, Y. Wang, Y. Wei, Y. He, Z. Yu, Z. Liu, L. Xu, ChemCatChem 6 (2014) 713–718.
[15] M. Choi, K. Na, J. Kim, Y. Sakamoto, O. Terasaki, R. Ryoo, Nature 461 (2009) 246–249.
[16] C. Jo, K. Cho, J. Kim, R. Ryoo, Chem. Commun. 50 (2014) 4175–4177.
[17] C. Jo, R. Ryoo, N. Žilková, D. Vitvarová, J. Čejka, Catal. Sci. Technol. 3 (2013) 2119–2129.
[18] W. Kim, J.C. Kim, J. Kim, Y. Seo, R. Ryoo, ACS Catal. 3 (2013) 192–195.
[19] J. Kim, M. Choi, R. Ryoo, J. Catal. 269 (2010) 219–228.
[20] E. Verheyen, C. Jo, M. Kurttepeli, G. Vanbutsele, E. Gobechiya, T.I. Korányi, S. Bals, G.V. Tendeloo, R. Ryoo, C.E.A. Kirschhock, J.A. Martens, J. Catal. 300 (2013) 70–80.
[21] J. Kim, W. Kim, Y. Seo, J.C. Kim, R. Ryoo, J. Catal. 301 (2013) 187–197.
[22] W. Kim, R. Ryoo, Catal. Letters 144 (2014) 1164–1169.
[23] Y. Seo, K. Cho, Y. Jung, R. Ryoo, ACS Catal. 3 (2013) 713–720.
[24] C. Perego, S. Peratello, Catal. Today 52 (1999) 133–145.
[25] M. Kolkowski, F.J. Keil, C. Liebner, D. Wolf, M. Baerns, J. Chem Eng, 108 (2005) 219–226.
[26] A. Zheng, S.-J. Huang, S.-B. Liu, F. Deng, Phys. Chem. Chem. Phys. 13 (2011) 14889–14901.
[27] X. Sun, S. Mueller, H. Shi, H. Shi, G.L. Haller, M. Sanchez-Sanchez, A.C. van Veen, J.A. Lercher, J. Catal. 314 (2014) 21–31.
[28] D.M. McCann, D. Lesthaeghe, P.W. Kletnieks, D.R. Guenther, M.J. Hayman, V.V. Speybroeck, M. Waroquier, J.F. Haw, Angew. Chem. Int. Ed. 47 (2008) 5179–5182.
[29] M. Zhang, S. Xu, Y. Wei, J. Li, J. Chen, J. Wang, W. Zhang, S. Gao, X. Li, C. Wang, Z. Liu, RSC Adv. 6 (2016) 95855–95864.
[30] B.T.L. Bleken, D.S. Wragg, B. Arstad, A.E. Gunnæs, J. Mouzon, S. Helveg, L.F. Lundegaard, P. Beato, S. Bordiga, U. Olsbye, S. Svelle, K.P. Lillerud, Top. Catal. 56 (2013) 558–566.